ADVANCED THERAPEUTICS
www.advtherap.com

Modulating Myeloid Immune Cell Migration Using Multivalently Presented Monosaccharide Ligands for Advanced Immunotherapy

Isabella Tavernaro, Alberto Marti Rodrigo, Maja Kandziora, Sabine Kuntz, Jens Dernedde, Christian Trautwein, Frank Tacke, Ana Blas-Garcia, and Matthias Bartneck**

Due to their importance for the outcome of the inflammatory response, the motile myeloid cells are a focus of novel treatment options. The interplay of selectins and their ligands with leukocytes and endothelial cells, which mediate endothelial attachment and transmigration of immune cells, can be modulated by selectin-binding structures. Here, a library of selectin-targeting ligands coupled to either gold, silver, iron oxide nanospheres, or quantum dots of 5–10 nm in size is used to systematically study their impact on immune cell motility. The multivalent presentation of the carbohydrate mimetics results in very low sub-nanomolar binding to L-selectin. Using human primary monocytes, granulocytes, lymphocytes, and macrophages, it is shown that the ligands exhibit only minor effects on uptake, whereas the motility of leukocytes is critically affected as observed in migration assays evaluated by flow cytometry. The carbohydrate mimetic ring structure, sulfation, in particular, and the degree of ligand presentation, are constituents which cohere in this process. Specific carbohydrate ligands can thus selectively regulate leukocyte subsets. These data form the basis for advanced immunotherapy which inhibits the amplification of inflammation by restricting leukocyte influx to injured tissue sites. Furthermore, the targeting ligands may complement existing treatment options for inflammatory diseases.

1. Introduction

1.1. Roles of Specific Immune Cells in Inflammatory Diseases

Immune cells patrol the blood and clear it from invading pathogens and foreign materials. Upon inflammation of an organ, leukocytes are recruited to migrate from the blood stream into the tissues. The neutrophils are the most numerous type of circulating immune cell and range from 50–70% of the blood leukocytes. Under homeostatic conditions, 10^9 neutrophils per kilogram of body weight per day egress from the bone marrow.[1] Neutrophil granules cover a collection of repository organelles on the one hand, and on the other, include toxic substances with diverse functions and relevance for the development of inflammatory sites.[2] Neutrophils impact on inflammation by their secretion of inflammation-related molecules such as the soluble urokinase plasminogen activator receptor (suPAR), which has

Dr. I. Tavernaro[+]
Institute of Inorganic and Analytical Chemistry
Justus-Liebig-University Giessen
Heinrich-Buff-Ring 17 35392 Giessen, Germany
E-mail: Isabella.Tavernaro@leibniz-inm.de
A. M. Rodrigo, A. Blas-Garcia
Dpto.Farmacología
Facultad de Medicina
Avda Blasco Ibañez n.15-17, 46010 Valencia, Spain

The ORCID identification number(s) for the author(s) of this article can be found under https://doi.org/10.1002/adtp.201900145

[+]Present address: INM-Leibniz Institute for New Materials, Campus D2 2, 66123 Saarbrücken, Germany

DOI: 10.1002/adtp.201900145

Dr. M. Kandziora
Institute of Chemistry and Biochemistry
Freie Universität Berlin
Takustraße 3, 14195 Berlin, Germany
Dr. S. Kuntz
Institute of Nutritional Sciences
Justus-Liebig-University Giessen
Wilhelmstraße 20, 35392 Giessen, Germany
Dr. J. Dernedde
Institut für Laboratoriumsmedizin, Klinische Chemie und Pathobiochemie
Charité-Universitätsmedizin Berlin
Augustenburger Platz 1, 13353 Berlin, Germany
Prof. F. Tacke
Department of Hepatology & Gastroenterology
Charité-Universitätsmedizin Berlin
Augustenburger Platz 1, 13353 Berlin, Germany
Prof. C. Trautwein, Dr. M. Bartneck
University Hospital Aachen
Pauwelsstraße 30, 52074 Aachen, Germany
E-mail: mbartneck@ukaachen.de

been closely linked to disease severity in systemic inflammatory diseases.[3]

Monocytes are another type of circulating leukocytes, which differentiate into the larger, less mobile, and long-lived macrophages which are known for their efficient phagocytosis. Macrophages reside in different tissues and are frequently the first cells to encounter foreign materials in tissue. Importantly, macrophages are functionally linked with neutrophils, with apoptotic neutrophils triggering a healing macrophage subtype.[4] We have shown before that modulation of selectins critically affects the outcome of hepatic inflammatory disease.[5]

Lymphoid cells, which are less efficient in the uptake of organic and inorganic nanomaterials in vitro and in vivo,[5–8] also contribute to inflammatory diseases such as sepsis and lymphopenia. Lymphocyte dysfunction can affect the prognosis in patients with critical illness or sepsis.[9] Understanding the applicability of nanomaterial physicochemistry and functionalization to control immune cells migration therefore is a key toward novel anti-inflammatory immunotherapies.

1.2. Role of Carbohydrates and Selectins in Leukocyte Migration

Leukocyte extravasation, the process in which blood cells migrate from blood into the tissues, is guided by a sequence of different signal proteins expressed by the endothelial cells. The first molecular guiding molecules the cells recognize are the selectins, whereas integrins appear at a later stage of the process.[10] There are three different types of selectins. All are composed of three calcium-dependent type I transmembrane glycoprotein receptors and an extracellular lectin domain, which bind to sialylated and fucosylated glycoprotein ligands. P-selectin is located on activated platelets as well as on the endothelium. E-selectin is exposed on the endothelium after activation by cytokines, and L-selectin is expressed by leukocytes. Therefore, selectins are potential targets for treatment of inflammatory diseases: targeting P- and E-selectins can be done to modulate endothelial cells, whereas an engagement of L-selectin enables to visualize or render the functions of leukocytes. The natural ligands for selectins within the inflammatory cascade are glycoproteins. Sialyl Lewis^X (SLe^x) is the glycidic common structure in all the natural selectin ligands and binds their receptors through fucose, galactose, or sialic acid saccharides.

Sulfation was found decades ago to be usable as an easy to generate selectin modulator. Sulfated polysaccharides are important for cell migration and are expressed on the cell surface as well as by the extracellular matrix. They interact with many different sulfated polysaccharide-binding proteins, such as growth factors, cytokines, and proteases. It is known that the structure, molecular weight, sulfation intensity, positions of moieties, and organization of sulfated domains are important in this regard.[11] The therapeutic use of SLe^X and its derivatives is compromised by their complex synthesis; thus research has been continued to mimic its binding affinity to selectins. For instance, we recently studied four different selectin-binding glycopolymers composed of linear poly(2-hydroxypropyl)-methacrylamide (PHPMA). These constructs either contained the tetrasaccharide SLe^X or the individual carbohydrates fucose, galactose, and sialic acids in order to mimic the complex SLe^X binding motive.[12] Follow-up studies have demonstrated that the degree of migration inhibition obtained from human immune cell migration assays correlates with disease severity in models of liver inflammation.[5]

1.3. Strategies to Enhance Selectin-Binding Properties

Carbohydrate mimetics increasingly attract the interest of scientists. They have for instance been explored in the drug discovery field, or as homeopathic drugs. For instance, bimosiamose, an inhalable low-molecular-weight SLe^x mimetic, demonstrated clinical efficacy in pulmonary disease.[13] Rivipansel, a pan-selectin antagonist, has been employed in vaso-occlusive crisis of sickle cell disease.[14] Glucosamine is used as a non-prescriptional drug for treating joint pain and arthritis. It was recently shown to exert anti-inflammatory effects via disruption of the NLR family pyrin domain containing 3 inflammasome.[15] However, the effects of carbohydrate mimetics on immune cell migration are currently unknown and need further exploration.

It is well known that the binding affinity between individual carbohydrate ligands and their receptors is low, reflected by dissociation constants mostly in the millimolar range.[16] During the last two decades, the multivalency effect (cluster effect) has been revealed to be one of the most important factors that can help provide higher binding affinities and stability.[17–19] In naturally occurring carbohydrates, the weak monovalent binding is enhanced by a high number of receptors. These chemical interactions can collectively result in bonds that are, in many cases, significantly stronger than the mere addition of the corresponding individual interactions. In order to use the multivalency effect as a principle for organization and action, it is necessary to design structures that take the intrinsic affinity of each ligand into account, their distance, as well as their relative spatial orientation.[17]

Due to their large surface–to-volume ratio, nanoparticles are promising carriers for selectins or their ligands and can potentiate the level of valency in presentation. In a previous study, monovalent carbohydrate mimetics (mannose, mannan, or mannosamine moieties) were immobilized as ligands onto poly(D,L-lactide-*co*-glycolide (PLGA) nanospheres.[20] It was shown that these nanocarriers led to the activation of macrophages and production of pro-inflammatory cytokines. However, a potential drawback of these nanoparticulate carriers is their "huge" size (around 180 nm), compared to small molecules. The size particularly means a problem for cellular therapies, for instance, in case of liver disease where drugs have to pass the slits of the liver endothelium which are about 20–80 nm. Hence, in order to overcome this barrier, a significant size reduction enables to meet the specific requirements for liver cell targeting.

Therefore, the aim of this study is to establish a concept for modulating immune cell migration using small carbohydrate-based ligand nanoparticle conjugates (**Figure 1**). Since L-selectin is primarily expressed by immune cells,[21] we hypothesized that the efficiency of migration can be influenced by the binding of L-selectin with tailored ligand nanoparticle conjugates. To study this, we generated an amino carbohydrate derivative ligand library. The ligands which also included sulfated versions

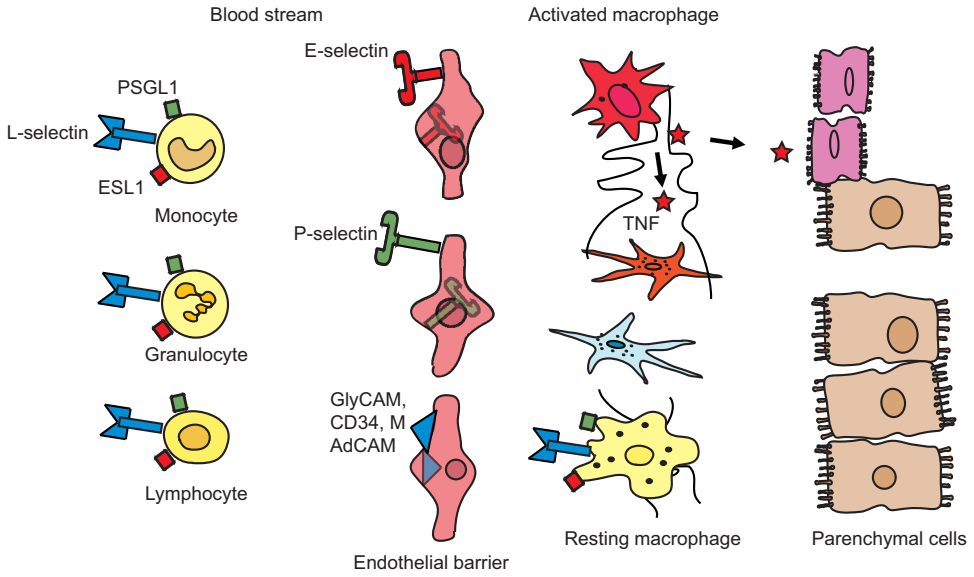

Figure 1. Role of carbohydrate ligands for immune cells. Selectins and their corresponding ligands are expressed by endothelial cells and immune cells in the liver. Inflammatory conditions evoke a rapid switch from the intracellular compartment to the outer part of the endothelial cell membrane. This regulation is here reflected by transparent and clean receptors. The inflammatory setting can potentially also activate hepatic stellate cells. These can be transformed into myofibroblasts that produce excess extracellular matrix. Macrophages, which have acquired pro-inflammatory activation, can secrete mediators such as the tumor necrosis factor (TNF) which potentially amplifies the inflammatory response.

were immobilized onto inorganic, spherical nanoparticles sizing 5–10 nm composed of either gold (AuNS), silver (AgNS), iron oxide (IONS), or semiconductor core-shell CdTe quantum dots (QD). We used human primary monocytes, granulocytes, lymphocytes, and macrophages to systematically study the effects of the nanocarrier material, sulfation, and particularly, the structure-binding relationships on cell migration. We used transwell assays as human cell based model for leukocyte migration and analyzed the cellular migration using flow cytometry.

2. Results and Discussion

Nanomedicines can evoke a specific binding to cellular receptors by making use of appropriate ligands. In particular selectins are interesting target molecules, since they critically influence inflammation by regulating the influx of immune cells from the blood into tissues. We have used selectin mimetics before to modulate immune cell migration in liver disease.[5] Generally, the binding properties of L-selectin can be improved by multivalent presentation and sulfation of ligands, but the use of sulfated carbohydrate mimetics is fairly unexplored since the understanding of their mode of action is limited. In previous studies, sulfation of multivalent glycopolymers resulted in strongly enhanced L- and P-selectin binding affinity.[22] Other studies have explored the potential of O-sulfated aminopyrans and poly(hydroxy)aminooxepanes as selectin inhibitors.[23,24] These studies demonstrated that the binding affinity to L-selectin increases with the epitopes' valency from monovalent epitopes like azidopyranes and azidoopexanes to their trivalent presentation.[24,25] It was determined that AuNS can be display 1000–5000 ligands on their surface, what results in even higher binding affinities at sub-nanomolar concentrations.[26]

We thus hypothesize that the specific design of the ligand nanoparticle conjugate is a critical parameter which not only defines the efficiency of selectin inhibitors but also strongly regulates immune cell motility. We thus generated different carbohydrate mimetics to verify our hypothesis. The synthesis was performed based on a known pathway using specific bicyclic 1,2-oxazine derivatives as key building blocks.[27,28] The reduction of the carbonyl group that is followed by the cleavage of the *N*-benzyl and N—O bonds leads to the transformation of the bicyclic 1,2-oxazine derivatives into the corresponding carbohydrate mimetics. Following this approach four different enantiopure aminopyrans,[27,29,30] which vary in their size, their number of hydroxyl groups, and their polarity, and one poly(hydroxy)aminooxepane,[25] which has a seven-membered polyhydroxylated oxacycle, were obtained (**Figure 2**A). In addition, commercially available glucosamine (GA) and mannosamine (MA) were used in this study.

2.1. Nanoparticle Syntheses and Characterization

For a multivalent presentation of these epitopes, syntheses of monodisperse nanoparticles (dispersity <10%) are necessary. In this study, we thus focused on inorganic nanoparticles with an inorganic particle core diameter below 10 nm. Compared to larger organic-based nanoparticles, the inorganic nanoparticles exhibit additional specific optical or magnetic properties. These properties can bring forth new desirable attributes, for example, the possibility to localize the particles in the body.[31] In addition, the

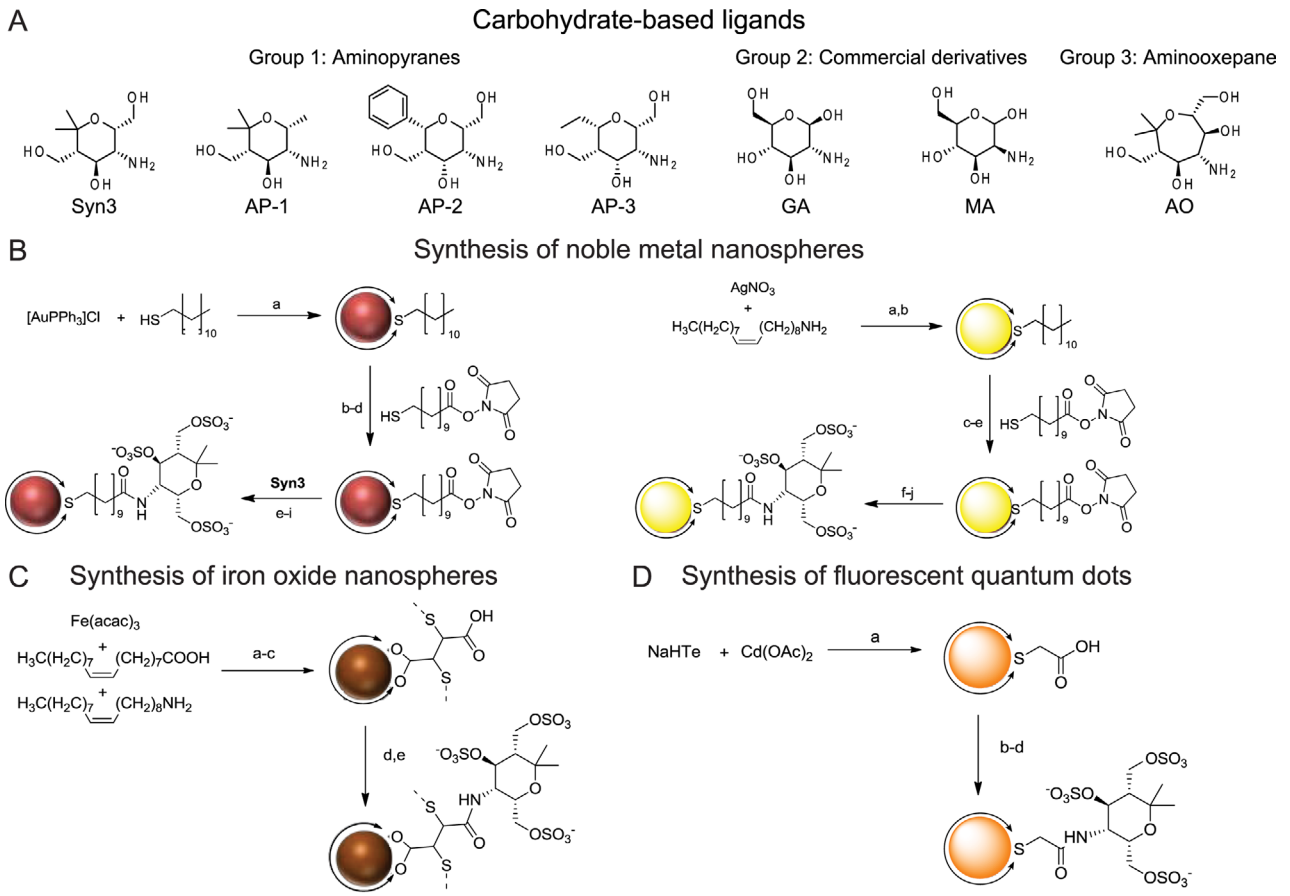

Figure 2. Synthesis of carbohydrate-coordinated nanospheres. A) Overview of the used epitopes in this study; synthesized aminopolyols (3-aminopyrans, group 1): (2S,3R,4S,5S)-3-amino-2,5-bis(hydroxymethyl)-6,6-dimethyltetra-hydro-pyran-4-ol (**Syn3**), (2S,3R,4S,5S)-3-amino-6,6-dimethyl-5-hydroxylmethyl-2-methyltetrahydro-pyran-4-ol (**AP-1**), (2S,3R,4R,5S,6R)-3-amino-2,5-di(hydroxyl-methyl)-6-phenyltetrahydro-2H-pyran-4-ol (**AP-2**), (2S,3R,4R,5S,6S)-(3-amino-6-ethyl-4-hydroxytetrahydro-2H-pyran-2,5-diyl)dimethanol (**AP-3**); group 2: commercially available glucosamine (**GA**) and mannosamine (**MA**) and the synthesized poly(hydroxy)aminooxepane (group 3) (2R,3S, 4R,5S,6S)-4-amino-2,6-bis(hydroxymethyl)-7,7-dimethyloxepan-3,5-diol (**AO**). B) Multistep synthesis approach of epitope-coordinated noble metal nanoparticles (Au and Ag), using the example of O-sulfated Syn3 epitope. Double arrows at the core represent the ligand shell completely surrounding the nanoparticles: AuNS a: $(CH_3)_3CHNH_2{\cdot}BH_3$, benzene, 1 h, 55 °C; b: $CHCl_3$/DMF, 30 min, r.t.; c: DMF, 18 h, r.t.; d: dialysis against DMF; e: DMF, 24 h, r.t., ethanolamine; f: dialysis against DMF; g: SO_3-DMF complex, DMF, 24 h, 0 °C → r.t.; h: dialysis against DMF; i: dialysis against H_2O; TMAH; AgNS a: $CH_3(CH_2)_7CH=CH(CH_2)_7COOH$, $(C_6H_5)_2O$,150 °C, 5 h; b: $CH_3(CH_2)_{11}SH$, r.t.; c: MUDHSE, hexane/DMF, r.t. 30 min; d: DMF, 24 h, r.t.; e: dialysis against DMF; f: Syn3, DMF, 30 min, r.t.; g: NEt3, 24 h, r.t., ethanolamine; h: dialysis against DMF; i: SO_3-DMF complex, DMF, 24 h, r.t.; j: dialysis against DMF and H_2O. C) Multistep synthesis approach of magnetic O-sulfated Syn3 coordinated iron oxide nanospheres (IONS). a: $CH_3(CH_2)_{13}COHCH_2OH$, $(C_6H_5CH_2)_2O$, 2 h, 200 °C → 1 h, 300 °C; b: DMSA, DMSO, 72 h, r.t.; c: dialysis against H_2O; d: O-sulfated Syn3, H_2O, NHS, EDC, 24 h, r.t.; e: dialysis against H_2O. D) Synthesis of fluorescent O-sulfated Syn3 coordinated quantum dots (QD). a: microwave irradiation; b: H_2O, NHS, EDC, 30 min, r.t.; c: O-sulfated Syn3, 2 h, r.t.; d: dialysis against H_2O.

small size of the particles supports targeting of cells in liver and other organs with opened endothelium, since smaller sizes improve tissue penetration.[32]

In order to systematically study the impact on leukocyte migration, we generated a library of carbohydrate-functionalized AuNS (Figure 2B). Further we immobilized the O-sulfated aminopyran (2S,3R,4S,5S)-3-amino-2,5-bis-(hydroxymethyl)-6,6-dimethyltetra-hydro-pyran-4-ol (Syn3) onto the surface of AgNS (Figure 2B), IONS (Figure 2C), and QD (Figure 2D) to study a potential influence of the particle type on cell migration. The physicochemical properties of the NS have been characterized in great detail using different characterization methods as shown in **Table 1**. The success of the postsynthetic modification steps was confirmed by nuclear magnetic resonance (NMR) and infrared (IR) spectroscopy (results and selected spectra are included in the supporting information, Sections 2 and 3). The particle sizes, morphologies, and the degree of agglomeration were studied by transmission electron microscopy (TEM) (**Figure 3**A). In addition, TEM micrographs confirmed the particle size and the degree of agglomeration in different solvents (data not shown). The hydrodynamic diameter of the nanoparticles was determined using dynamic light scattering (DLS) analysis. All synthesized nanoparticles exhibited a negative zeta potential (ζ-potential) ranging from −15.5 to −51.2 mV, indicating electrostatic stabilization through the highly negatively charged surface. To study the stability of the sulfated particles and the influence of the formation of a protein corona under relevant biological conditions, the hydrodynamic diameter (d_m) and

Table 1. Overview of physicochemical characterization of the nanoparticle library.

Nanoparticle type	Sulfated	d_{TEM} [nm]	d_h [nm]	ζ-potential [mV]	λ_{max} (UV–vis) [nm]
S-Syn3	+	6.8 ± 0.5 (7%)	13 ± 3 (20%)	−51.2 ± 5.9	526
S-AP-1	+	6.9 ± 0.4 (6%)	17 ± 3 (16%)	−45.6 ± 2.6	526
S-AP-2	+	6.9 ± 0.3 (4%)	25 ± 6 (23%)	−31.5 ± 0.6	530
S-AP-3	+	7.2 ± 0.2 (3%)	30 ± 5 (16%)	−32.0 ± 2.1	527
S-GA	+	7.1 ± 0.3 (4%)	15 ± 3 (17%)	−51.0 ± 1.5	523
S-MA	+	7.1 ± 0.3 (4%)	19 ± 4 (19%)	−44.5 ± 2.8	523
S-AO	+	6.7 ± 0.3 (5%)	29 ± 4 (15%)	−35.2 ± 3.5	530
AP-1	−	6.9 ± 0.4 (6%)	12 ± 2 (17%)	−19.7 ± 5.0	528
GA	−	7.1 ± 0.3 (4%)	12 ± 2 (17%)	−16.9 ± 3.2	524
MA	−	7.1 ± 0.3 (4%)	16 ± 3 (19%)	−15.5 ± 1.6	521
AO	−	6.7 ± 0.3 (5%)	23 ± 5 (22%)	−15.8 ± 2.4	526
S-Syn3 AgNS	+	4.8 ± 0.4 (8%)	22 ± 3 (13%)	−20.4 ± 2.2	433
S-Syn3 IONS	+	4.2 ± 0.4 (10%)	12 ± 3 (24%)	−39.6 ± 4.3	—
S-Syn3 QDs	+	5.0 ± 0.2(4%)	n.d.	−26.4 ± 2.9	592

To determine the particle diameter and the size distribution, the samples were characterized by TEM micrographs analysis (d_{TEM}: mean particle diameter as determined using transmission electron microscopy). The hydrodynamic diameter of the particles in H_2O (d_h) was measured by DLS using a number weighed distribution. Numbers in brackets indicate the size dispersity p. It is calculated by the formula $p = \sigma/\mu$ with σ being the standard deviation and μ as mean value. The surface charge of the nanoparticles was determined by ζ-potential measurements. Optical properties of AuNS, AgNS, and QDs were studied with UV–vis spectroscopy (λ_{max}: wavelength with maximum absorbance). n.d., not determined; "+", sulfated; "−", unsulfated.

the ζ-potential (ζ_m) of two sulfated AuNS (S-Syn3 and S-AP-1) were also measured in cell culture medium as physiological matrix which contains high amounts of salts, amino acids, and proteins (Figure S14 and Table S1, Supporting Information). For this purpose, the sulfated nanoparticles were incubated in cell culture medium with 10% fetal calf serum (FCS) for 24 h. Although larger hydrodynamic diameters were obtained in presence of medium, the content of agglomerates increased only slightly from 0.4% to 3.3% (S-Syn3) and 0.2% to 0.3% (S-AP-1), respectively. Thus, for both nanoparticle types, no significant agglomeration has been observed and the size increase can be assigned to the formation of a protein corona. The obtained results are in line with previous studies.[33,34] The observed decrease of the ζ-potential of the particles toward the average value of the medium proteins (less than −30 mV) supports these findings.

In summary, all synthesized nanoparticles were approximately spherical, indicated no agglomeration, and exhibited a narrow size distribution (<10%). Neither the postsynthetic functionalization steps nor the sulfation had an impact on these parameters. These results were also confirmed by absorbance measurements of the noble metal nanoparticles and quantum dots. Further UV–vis spectroscopy was used to control potential effects on the optical properties of AuNS samples (Figure 3B). The absorbance maximum of the particles was determined in a range of 520–530 nm and did not change significantly through the various postsynthetic steps. The magnetic properties of the iron oxide based particles were demonstrated to be typical superparamagnetic behavior with its loss of hysteresis (Figure 3C). The bright fluorescent QD exhibited a stable fluorescent signal which could be analyzed using appropriate methods (Figure 3D).

In order to facilitate strong binding affinities to L-selectin, the presence of a large numbers of ligands on the particle surface is mandatory. To quantify the number of ligands, we used thermogravimetric analysis of the nanoparticles. Thus, the loss of mass was recorded as a function of temperature (Figure S15, Supporting Information). This resulted in 8 ligands per nm^2 (AuNS), 4 ligands per nm^2 (IONS), and 6 ligands per nm^2 (QDs). The different NS types present 450–1200 ligands per particle, which is in the same order of magnitude compared to previous studies.[26,35]

2.2. L-Selectin Binding Properties

The binding activity to L-selectin plays a key role for understanding the interactions between selectin-binding nanospheres and cells.[5,12] A competitive surface plasmon resonance (SPR) binding assay was performed to study the potential binding interaction of the sulfated aminopyrans S-AP-1, S-AP-2, and S-AP-3 coordinated AuNS with L-selectin. All three sulfated samples were demonstrated to be very efficient inhibitors of the interaction of L-selectin to their natural ligands, with IC_{50} values in the high pM to low nM range (S-AP-1: 600 pM; S-AP-2: 1900 pM; S-AP-3: 1600 pM), which are substantial values in the field of selectin inhibitors. These data are in line with the obtained IC_{50} values of sulfated aminopyran and aminofuran functionalized AuNS from a previous study.[26] The increasing IC_{50} values from 350 pM (S-Syn3) to 1900 pM of S-AP-2 (with a sterically hindered phenol group) show that the arrangement of the negative charges on the particle surface in combination with the polyanionic structure of the ligands are decisive for a strong selectin–nanoparticle binding. Thereby, our data on the binding efficiency indicated not only a positive effect of the multivalent presentation of the ligands, but also an influence of the ligand structure on binding to L-selectin.

2.3. Endothelial Cell Viability

Endothelial cells decorate the blood vessels and potentially get into contact with nanospheres. In parallel, they represent the

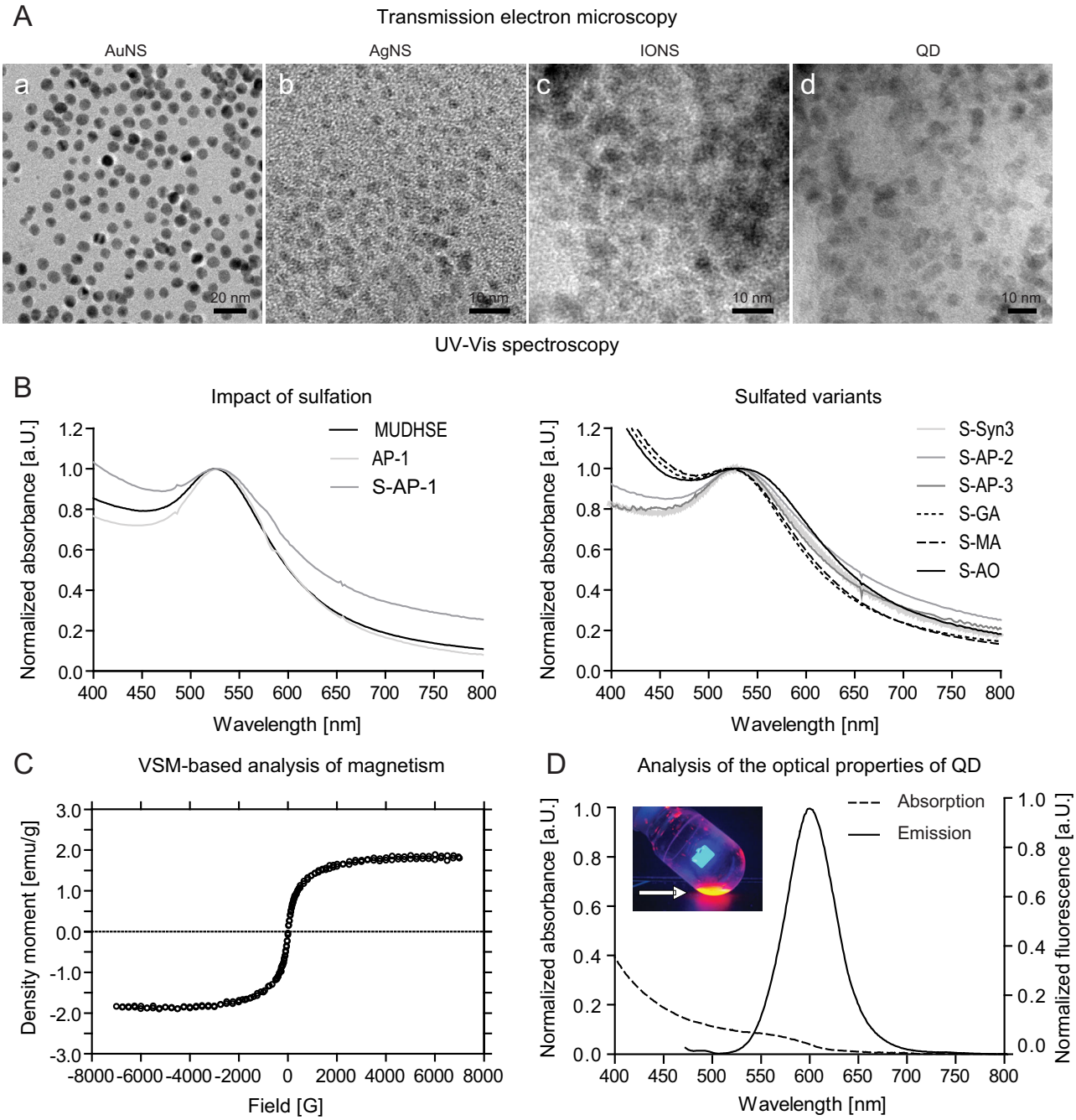

Figure 3. Characterization of nanoparticles and their unique properties. A) TEM micrographs of O-sulfated Syn3 functionalized nanospheres generated from gold, (Au, a), silver (Ag, b), iron oxide (IO, c), and quantum dots (QD, d). B) UV–vis spectroscopy based analysis of optical properties of gold nanospheres before and after the functionalization and sulfation steps. C) Vibrating-sample magnetometer (VSM) analysis of the magnetic properties of a representative IONS sample (DMSA-coordinated IONS). D) Examination of the fluorescent properties of O-sulfated Syn3 coordinated QDs, including an inset photo which demonstrated fluorescence intensity.

barrier immune cells have to pass in order to get to inflammatory sites. To study the biocompatibility of our carbohydrate mimetic coordinated nanoparticles with endothelial cells which get into contact with the NS because they line all blood vessels and express selectin and ligands (Figure 1), human umbilical vein endothelial cells (HUVEC) were incubated with the nanospheres at a concentration of 10 nM for 24 h. Potential effects of the NS on cellular proliferation or viability were assessed using an 3-(4,5-dimethylthiazol-2-yl)-2,5-diphenyltetrazolium bromide (MTT) assay. Independent of the sulfated aminopyran or aminooxepane ligand, the functionalized AuNS exhibited no significant effects on the endothelial cells at the particle concentrations of 10 nmol L^{-1} (Au content: 20 µg mL^{-1}). We have further systematically exchanged the core material,

S-Syn3-AgNS (Ag content: 4 μg mL^{-1}), S-Syn3-IONS (Fe content: 0.9 μg mL^{-1}), and S-Syn3-QDs (Cd content: 0.5 μg mL^{-1}) (Figure S3, Supporting Information). We have also performed a SYTOX Green Dead Cell Stain at tenfold lower (0.1 nM for AuNS) and tenfold higher (100 nM for AuNS) concentrations of the particles (data not shown). Reduction of viability was noted for the AgNS only, corroborating earlier findings on the cytotoxicity of AgNS, particularly in the size range of 10 nm.[36]

Thus, neither the substitution pattern at the pyran ring (S-Syn3 or S-AP-1) nor the ligand type (aminopyran or aminooxepane) and the core material (AuNS, AgNS, IONS, QD) had a negative impact on the biocompatibility of the sulfated NS. These findings allowed us to conclude that the cellular binding of the sulfated carbohydrate mimetic coordinated NS does not interfere with the viability of endothelial cells.

2.4. Effects of AuNS-Coupled Endgroups on Leukocyte Uptake and Migration

It is crucial to close the knowledge gaps between the role of multivalent presentation of selectin inhibitors and cellular functionality. Hence, we further studied the impact of the different parameters on leukocyte motility. It is particularly promising to modulate immune cell motility since these cells migrate into inflammatory sites, where they can amplify the inflammatory reaction. Therefore, we performed assays for determining leukocyte migration in vitro, which has important implications for the in vivo effects of the particles. We have demonstrated earlier that these effects on immune cell migration in vitro correlate with in vivo effects in models of inflammatory liver injury.[5,12] We incubated the cells with AuNS at a particle concentration of 10 nM (Au content: 20 μg mL^{-1}) for 60 min. Subsequently, the cells were subjected to an established assay for immune cell migration, which is based on membranes with 5 μm sizing pores (model endothelium) which immune cells can only pass upon active processes (**Figure 4**A). We used flow cytometry to discriminate immune cell subsets based on their size (forward scattering light area, FSC-A) and granularity (sideward scattering light area, FSC-A), as illustrated by representative plots, here of cells which did not migrate. The green gate in the graphic depicts the selection of granulocytes which exhibit comparatively high SSC-A, as well as lymphocytes (orange gate) and monocytes (red gate) (Figure 4B). The uptake of the AuNS by leukocytes was quantified using inductively coupled plasma mass spectrometry (ICP-MS), using established methods.[37] These analyses demonstrated that the amount internalized by the cells was increased by all types of functionalization, except for AP-1. Yet, these data demonstrated no statistical differences (Figure 4C). The modulation of selectins represents a key tool to critically modulate immune cell migration. We therefore used flow cytometry to further count the numbers of migrated immune cells and to determine the effects on the numbers of each subset (Figure 4D). Statistical quantifications of numbers of migrated cells revealed significant effects on the total number of migrated leukocytes; in particular, sulfated Syn3, as well as the sulfated variants of AP-1 and AP-2, reduced migration. These very important effects on the whole leukocyte fraction is mainly owed to effects on neutrophils. Monocytes demonstrated particular responsivity to both aminooxepane ligand functionalized NS, AO, and S-AO, suggesting a particular role of these seven-ring ligands. Interestingly, S-AP-3 led to increased leukocyte cell numbers, which was mainly based on accelerated lymphocytes for which the induction of migratory activity was significantly elevated. The migration of monocytes and lymphocytes, which both form the peripheral blood mononuclear cells (PBMCs), were specifically reduced S-AO (Figure 4E).

These data clearly demonstrate that the selectin inhibitors exert their effects through binding to immune cells, rather than by being taken up by them, which is in accordance to earlier findings.[5,12] Thus, these effects on cell mobility occur much more rapid than molecular reprogramming of cells, that is, by selective drugs. Sulfation has a critical impact on leukocyte migration, but also the polyanionic structure of the ligands in combination with the arrangement of the negative charges on the particle surface play an important role for the effects on immune cells. S-Syn3, S-AP-1, and S-AP-2 appear to be most suitable in their presentation of sulfate groups to inhibit leukocyte migration. Nevertheless, there are several specific properties of the different blood immune cells which lead to differences in their migratory behavior. These differences can assumingly also be led back to differences in the expression of L-selectin by these cells, which is critically regulated in disease.[38]

Interestingly, neutrophils were further strongly affected by also two other sulfated molecules, S-AP-1 and S-AP-2. Since both aminopyrans differ from each other in their number of sulfate groups and their substitution at C1, the spatial orientation of the sulfate groups seems to be important for the inhibition of neutrophil migration. Thus, this information might be used to develop novel treatment options by targeting neutrophil granulocytes in inflammatory liver disease or COPD. Neutrophils exhibit a multitude of important functions to protect the human body, that is, they perform phagocytosis to remove pathogens, generate reactive oxygen species (ROS), and degranulate many other compounds such as sticky web-like structures composed of chromatin filaments and proteins, which are defined as neutrophil extracellular traps (NETs).[39] These NETs can also immobilize nanoparticles extracellularly, dependent on the charge of the particles.[7]

In neutrophil-directed therapies, they are mobilized to improve the health status of patients suffering from leukopenia, for instance, by using the recombinant granulocyte colony-stimulating factor filgrastim (G-CSF and CSF-3).[40] The continuous influx of neutrophils in large numbers during acute inflammatory settings exhibits a huge, yet mostly unexplored potential for interventions. Novel nanotherapies might bear the ability to modulate neutrophil migration, which might then be combined with filgrastim. Interestingly, there was a tendency of S-AP-3 to further increase the mobility of neutrophils.

2.5. Impact of the Core Material on Leukocyte Migration

In order to further study the influence of the core material on the binding capabilities of the conjugated ligands, we used AgNS, IONS, and semiconductor QD to immobilize the biologically active sulfated Syn3. The fluorescent signal of the QD can be used to study the uptake by different immune cells. Similar to earlier findings, monocytes were most efficient in the uptake of QD,

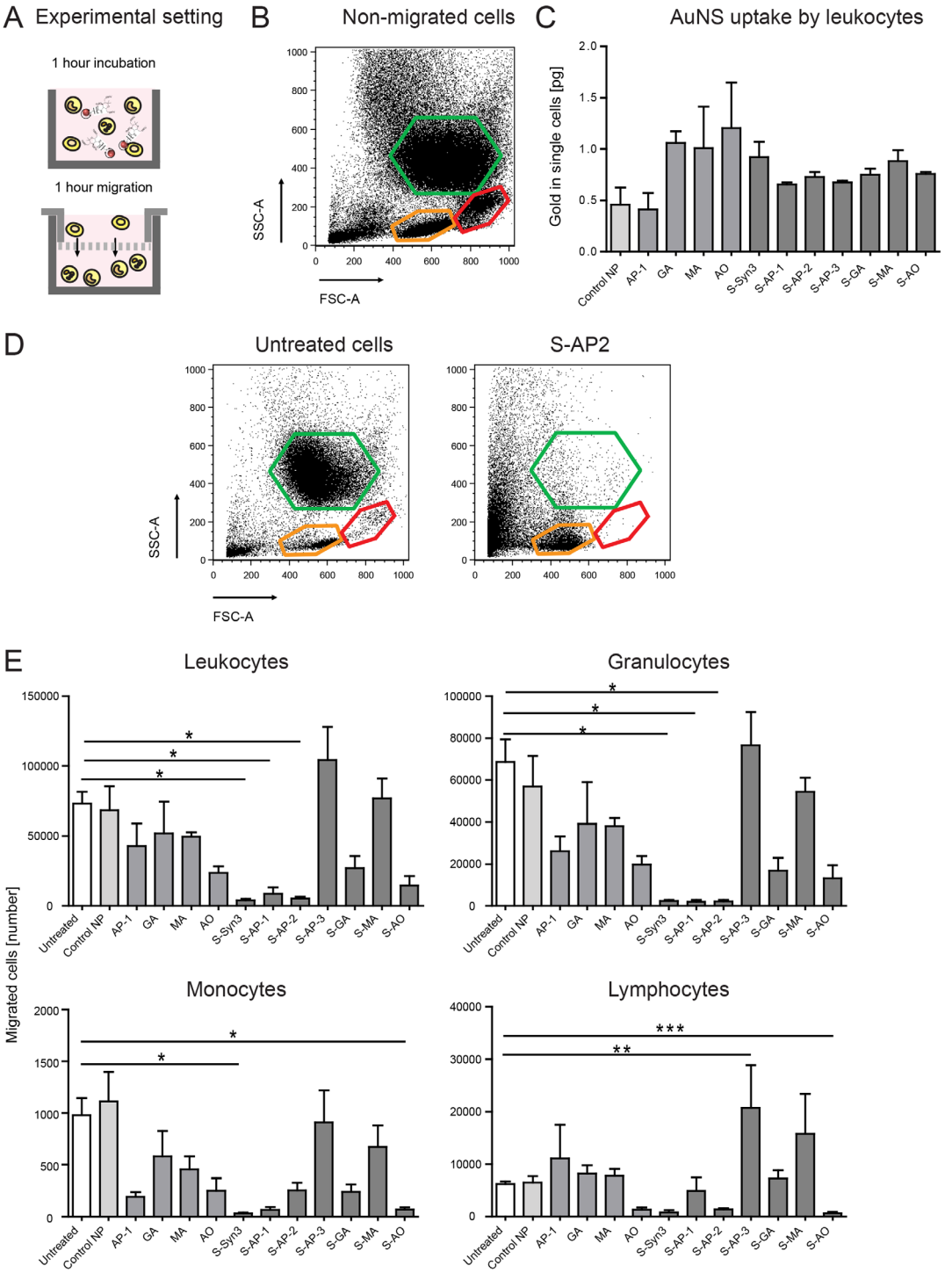

Figure 4. Effects of ligand shell sulfation on leukocytic uptake and impact on cellular migration. A) Experimental setting for the combined analysis of uptake and cell migration. Human primary blood leukocytes, namely granulocytes (green selection), monocytes (red selection), and lymphocytes (orange selection) were isolated from human blood using dextran sedimentation. Two million cells were incubated in RPMI1640 with 5% fetal calf serum with nanoparticles at 10 nM for 60 min and left to migrate through 5 µm sizing meshes. Control cells were untreated migrated cells, and control particles were functionalized with sulfated 11-mercaptoundecanol (MUDS). Various aminopyran-based endgroups were used: aminopyran 1 (AP-1), glucosamine (GA), mannosamine (MA), aminooxepane (AO), sulfated Syn3 (S-Syn3), sulfated aminopyran 1 (S-AP-1), sulfated aminopyran 2 (S-AP-2), sulfated aminopyran 3 (S-AP-3), sulfated glucosamine (S-GA), sulfated mannosamine (S-MA), sulfated aminooxepane (S-AO). B) Representative flow cytometric plot used for analysis of uptake or for follow-up migration assay. C) The NS uptake after 60 min as quantified using ICP-MS. D) Representative plots for the application of flow cytometry for quantification of the cells which migrated to the bottom of the Boyden chamber. E) Statistical evaluation of the flow cytometric uptake of NS with the different modifications. Mean data of $n = 4$. $^*p < 0.05$ (one way ANOVA).

as evidenced by the fluorescent signal of the QD analyzed using flow cytometry, as indicated by a shift in the fluorescent signal in signal overlays, when compared to that of granulocytes and lymphocytes, which did not show this signal shift (**Figure 5**A). Corroborating with the findings on the induction of increased uptake by coupled groups, the Syn3 ligands also increased the uptake of AgNS and IONS by leukocytes as measured using ICP-MS (Figure 5B). The Syn3 ligand was similarly efficient when immobilized to the QD, which became clear in flow cytometric scatter plots (Figure 5C). Flow cytometric analyses and statistical quantifications of the impact of the different Syn3 carrying materials demonstrated that the QD- immobilized sulfated Syn3 inhibited monocyte migration almost significantly (Figure 5D). The AgNS generally had a minor impact on leukocyte migration (Figure 5E). The sulfated Syn3 conjugated IONS exhibited a significant inhibition of monocyte migration, but not of the other immune cells (Figure 5F).

The AgNS exhibited, compared to the AuNS, very limited effects on the leukocytes. The knowledge on the reason for the cytotoxicity of silver nanoparticles is quite limited, but it was shown by others that specifically small-sized silver nanoparticles around 10 nm can exert cytotoxic effects.[36] Additional sources for silver cytotoxicity is currently being investigated by other groups and their data indicate an induction of ROS and a release of Ag ions as chemical causes for the toxicity. The iron-oxide-based nanoparticles reproduced the effects of the AuNS in the clearest fashion as indicated by a significant reduction in monocyte migration (Figure 5E). Iron oxide such as Feraheme (ferumoxytol) is approved for treatment of anemia. However, iron oxide might, at higher dosages, lead to an activation of immune cells based on the iron overload.[41]

In summary, these data suggest that the particle core material plays rather a minor role and an efficient epitope such as Syn3 can be immobilized on the particle surface of various nanoparticles to facilitate inhibition of immune cell migration. Thus, the inhibition of migration might further be combined with particles which exhibit other properties resulting from their composition material which may enable fluorescence (QD) and magnetism (iron oxide). These data demonstrate that particularly Syn3 with the three sulfate groups and its specific substitution pattern at the six-membered ring inhibits the migration of both types of phagocytic blood immune cells (monocytes and neutrophils) most efficiently. The combined inhibition of monocyte and neutrophil migration by Syn3 could be a promising option for advanced therapies since by targeting both cell types in therapies in parallel. This could prevent compensatory activities of both cell types; it has been reported that neutrophils can compensate the functions of monocytes if the latter are inhibited. This is not only important in inflammatory disease settings, but it is also known that in different types of tumors, fibroblasts compensate a depletion of macrophages by activating neutrophils[42]

However, the material also plays an important role for the interaction with the cellular receptors and leads to the assumption that gold and iron oxide based materials possess the highest potential to explore novel concepts for immunomodulation. The silver-based NS slightly reduced cellular viability of endothelial cells and also reduced the numbers of the immune cell effects. This material is rather suitable for use in anti-bacterial coating than in biomedical applications since it might harm various other cell types as well if it would be used in vivo. The QDs evoked a high level of standard deviation between different donors, yet had an almost significant inhibition of monocytes, which might be worth studying further. However, drawbacks of QDs are their composition, using heavy metals such as cadmium and tellurium, as well as the difficult synthesis. Consequentially, gold appears to be suited best to study the sensitive interactions of immune cells with different surface groups because it is non-toxic and not present in the body (unlike iron, which is present in the body).

2.6. Impact on Macrophage Migration

Based on the results from leukocyte migration, we used selected nanoparticles to study the effects on human primary macrophages, which are long-lived cells derived from monocytes or specific stem cells.[43] We used a similar transwell migration assay, but the macrophages were left to migrate for a longer period of 16 h compared to the 1 h incubation of the blood immune cells (**Figure 6**A). The longer incubation time for the migration assays is based on our own earlier studies, which demonstrated a strongly reduced migratory activity of macrophages than blood monocytes.[44] The uptake experiment was also performed for 60 min, in order to be comparable to the experiment with leukocytes as shown above (Figure 4C). The uptake of the AuNP with the different ligands was not significantly affected by the different ligands (Figure 6B). Interestingly, S-Syn3 increased the uptake of AgNS and IONS, yet did not reach significance (Figure 6C). We also evaluated the migratory activity of the macrophages using statistical analyses and we noted a strong impact of the different ligands on the mobility of macrophages. Interestingly, many types of material such as glucosaminoglycan as ligand inhibited the migration of macrophages, nearly irrespective of sulfation, as displayed in statistical enumerations, except for S-GA (Figure 6E). While S-Syn3 increased the NS uptake by macrophages, it also significantly reduced the migration of macrophages when coupled to silver or iron oxide. The QD showed a similar inhibition which, however, did not reach statistical significance (Figure 6F).

The sulfation might therefore change the normal properties of GA which inhibits inflammatory activation of macrophages.[15] These effects of GA sulfation might be useful to prevent binding to macrophages by a currently unknown mechanism. Preventing targeting macrophages might be interesting for many other types of applications in which lymphocytes or hepatic stellate cells are intended to receive the cargo of a drug carrier. It might be led back to an interaction with or due to an interaction with the CD47 "Don't eat me" ligand. A blockage of CD47 was recently shown to stop tumor progression. By binding to CD47 on cancer cells, these are much more rapidly eliminated and are more prone to be eliminated by macrophages.[45] Our small-sized molecule might thus use a route which leads to a similar effect and thus certainly is of interest to researchers in immunotherapy.

2.7. Concentration-Dependent Inhibition of Cell Migration

Due to the well-defined effects of the AuNS on the immune cells, we further studied their effects in a dose-dependent fashion.

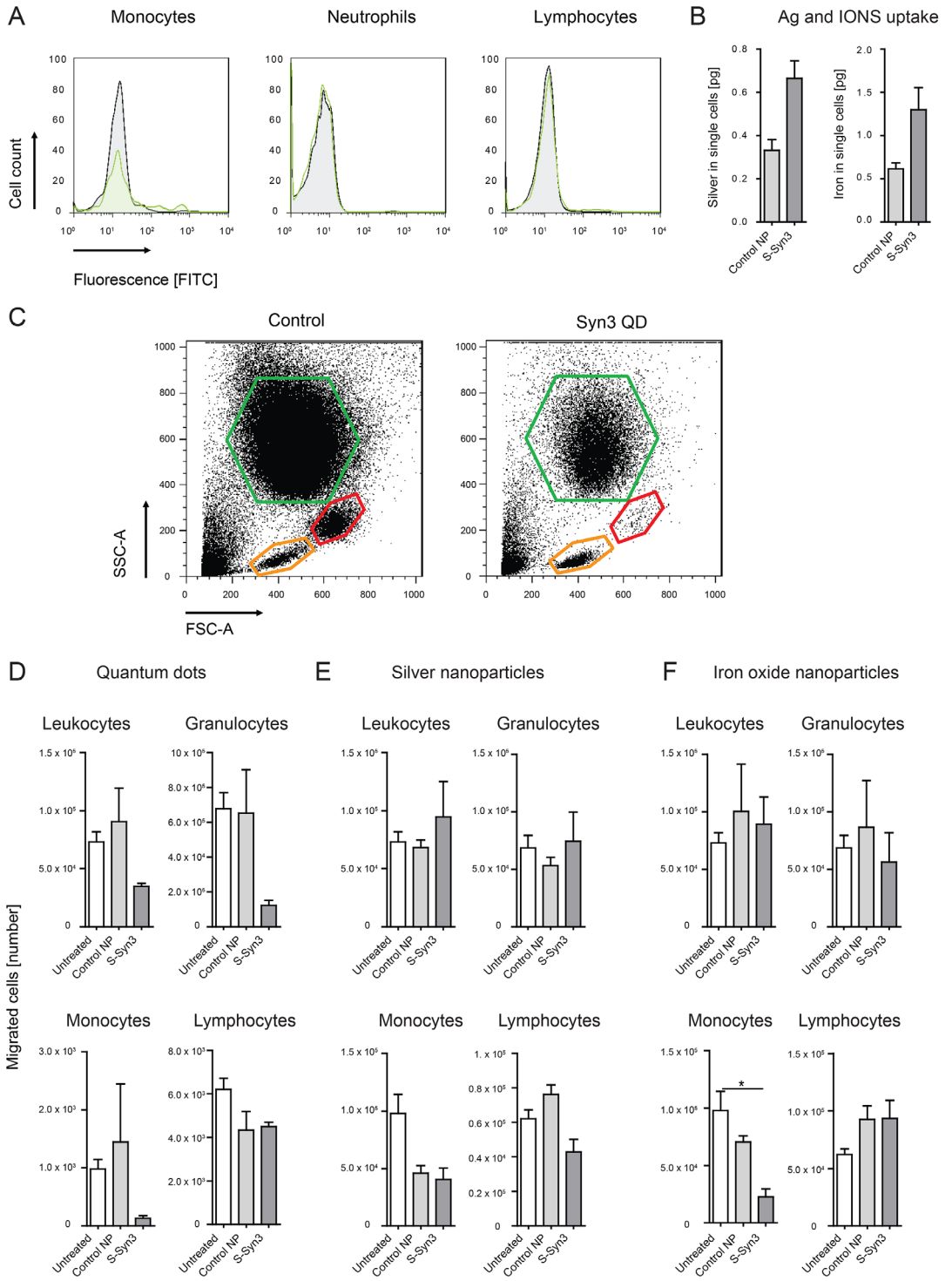

Figure 5. Effects of functionalized fluorescent quantum dots, iron oxide, and silver NS on immune cells migration. Human primary leukocytes were isolated from human blood using dextran sedimentation. Two million cells were incubated in RPMI1640 with 5% fetal calf serum with nanoparticles at 10 nM (Cd content: 0.5 µg mL^{-1}) for 60 min and left to migrate through 5 µm sizing meshes. A) Representative flow cytometric overlays (grey: control, green: QD) for the quantification of QD uptake by the QD fluorescence in cells. B) The uptake of different QD by human primary blood leukocytes (monocytes, granulocytes, and lymphocytes) as quantified by ICP-MS. C) Representative flow cytometric scatter plots of the analysis of leukocyte migration as influenced by preincubation with Syn3-coordinated QD. Granulocytes (green selection), monocytes (red selection), and lymphocytes (orange selection). D) Statistical quantification of changes in cell migration evoked by sulfated Syn3 coupled to CdTe/ZnS QDs; QDs decorated with mercaptohexanoic acid (MHA) or Syn3. E) Effects of the sulfated Syn3 ligand coordinated to AgNS compared to citrate decoration. F) Effects of Syn3 coupled to iron oxide nanoparticles. 2,3-dimercaptosuccinic acid (DMSA)-functionalized IONS have been used as control NS. Mean data of $n = 4$. *$p < 0.05$ (one way ANOVA).

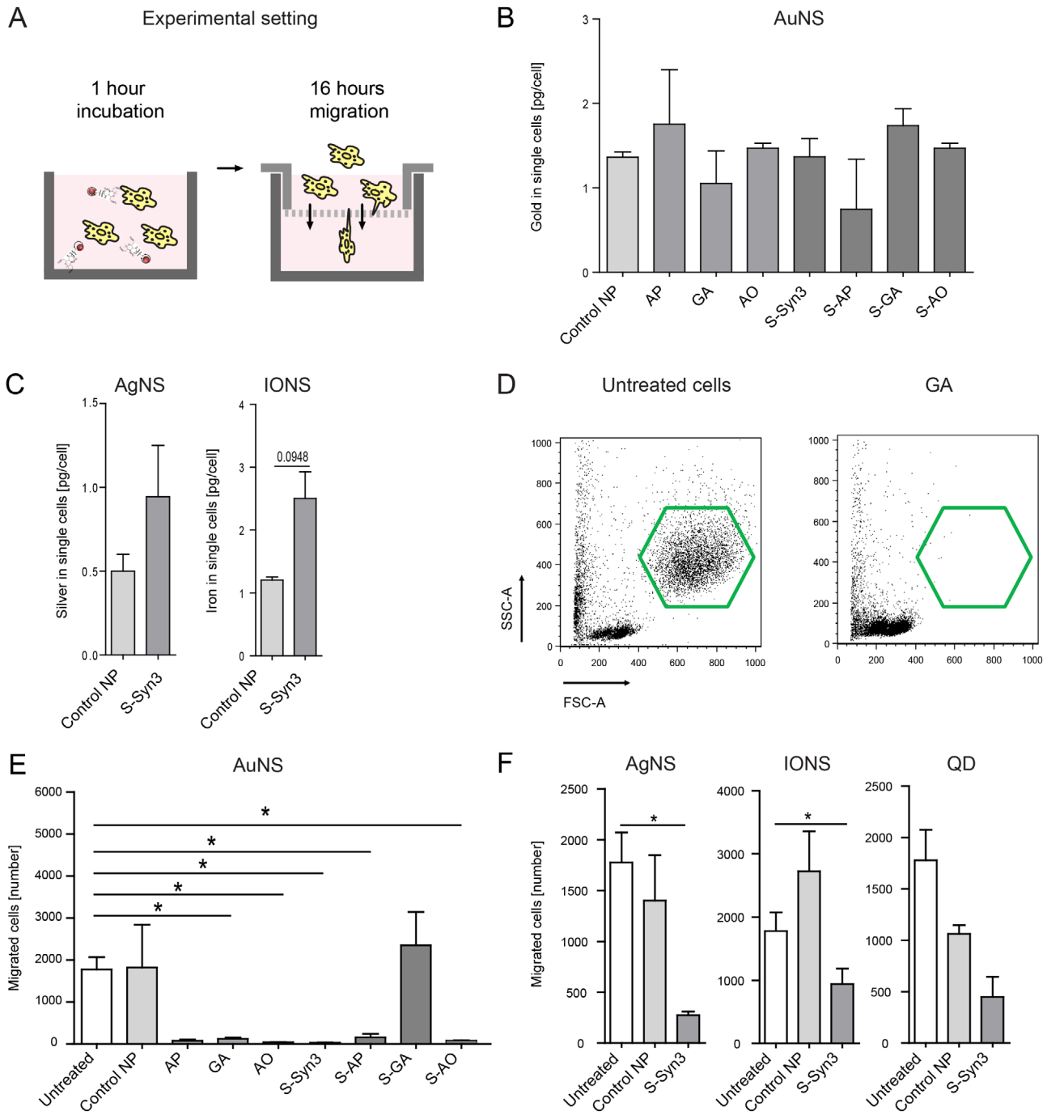

Figure 6. Effects of carbohydrate-functionalized NS and ligand shell sulfation on macrophage migration and uptake. Human primary monocytes were generated from blood mononuclear cells and macrophages were harvested after 7 days of cultivation. A) One million cells were incubated with AuNS functionalized with either sulfated 11-mercaptoundecanol (MUDS) (as the control ligand) or the carbohydrate mimetics; the aminopyran-based end-groups were unsulfated AP-1, unsulfated GA, sulfated Syn3 (S-Syn3), sulfated AP-1 (S-AP-1), sulfated AP-2 (S-AP-2), sulfated GA (S-GA), or sulfated aminooxepane (S-AO) at 10 nM for 60 min and left to migrate for 16 h. B) ICP-MS-based analysis of the uptake of the different AuNS and C) of iron oxide and AgNS by macrophages. D) Representative flow cytometry plots. E) Statistical quantification of macrophage migration (green gate) using flow cytometry. F) Effects of other material classes on macrophage migration. Mean data of $n = 4$. *$p < 0.05$ (one way ANOVA).

These data demonstrate that Syn3 is particularly potent even at very low particle concentrations of 1 nM (Au content: 2 μg mL^{-1}), where effects were significant, similar to 10 nM (Au content: 20 μg mL^{-1}) which were used for the previous experiments. It may thus be added at different amounts and be efficient at any concentration. However, the effects on leukocyte migration at a particle concentration of 100 nM (Au content: 195 μg mL^{-1}) were so strong that few migrated cells were found. The inhibitory effect of GA on total leukocytes showed a clear trend toward concentration dependency. The AgNS, unexpectedly, led to even increased cell numbers when sulfated Syn3 was immobilized to them, whereas at the highest concentration of 100 nM (Ag content: 38 mg mL^{-1}), cells were absent, probably owing to toxic effects of Ag-based carriers in this size range[36] (**Figure 7**A). The data on the neutrophil migration depicted mostly the trend for the total leukocytes, which they are a main part of, and further revealed a significant inhibitory effect on their migration at 100 nM (Fe content: 8 μg mL^{-1}) S-Syn3@IONS (Figure 7B). The effects of different materials at different sizes were remarkable for the monocytes. While most particles reduced their migration, in many cases, significantly, the lower concentrations of AuNS or AgNS even increased their numbers. Thus, the monocytes were probably most responsive to the materials (Figure 7C).

These findings are in good agreement with earlier data of own studies in which monocytes were shown to be the most important cells for AuNS uptake, both in vitro and in vivo.[6,8] The effects of the different types of particles and concentrations did only result in slight changes in lymphocyte numbers and low concentrations of AgNS and IONS increased their number. This increase in numbers might be explained by a stimulation of their migration as mediated by the phagocytic immune cells (granulocytes and monocytes). Thus, lymphocytes were the cell type least responsive to the materials, which is similar to earlier own studies on AuNS in vitro and in vivo.[6,8]

3. Conclusions

Immunomodulation is receiving tremendous attention from the scientific community from various areas of applications. Traditional medicines are hampered by systemic side effects. We have unraveled several novel selectin ligands which might be used to specifically modulate the migration of immune cells. Hence, our data strongly improve the understanding of carbohydrates for functionalizing nanospheres for selective modulation of immune cell subsets. Thereby, we provide an update on the role of the valency and structure of selectin-targeting ligands in immunomodulation.

Nanomedicines offer a size minimization, but often times are much larger than small molecules, thereby actually losing the advantages of size minimization. Here, we have presented a collection of small bioactive nanocarriers of four different types of material with particle core sizes below 10 nm. We consider this low size to be the lower limit for an efficient exploitation of the multivalency effect. Our results indicate a higher impact of the organic ligand shell than the inorganic core materials. Our data demonstrate that the aminopyran ligands facilitate highly specific binding to different immune cell subsets, resulting in more pronounced effects in vitro. This nanosphere library evokes a

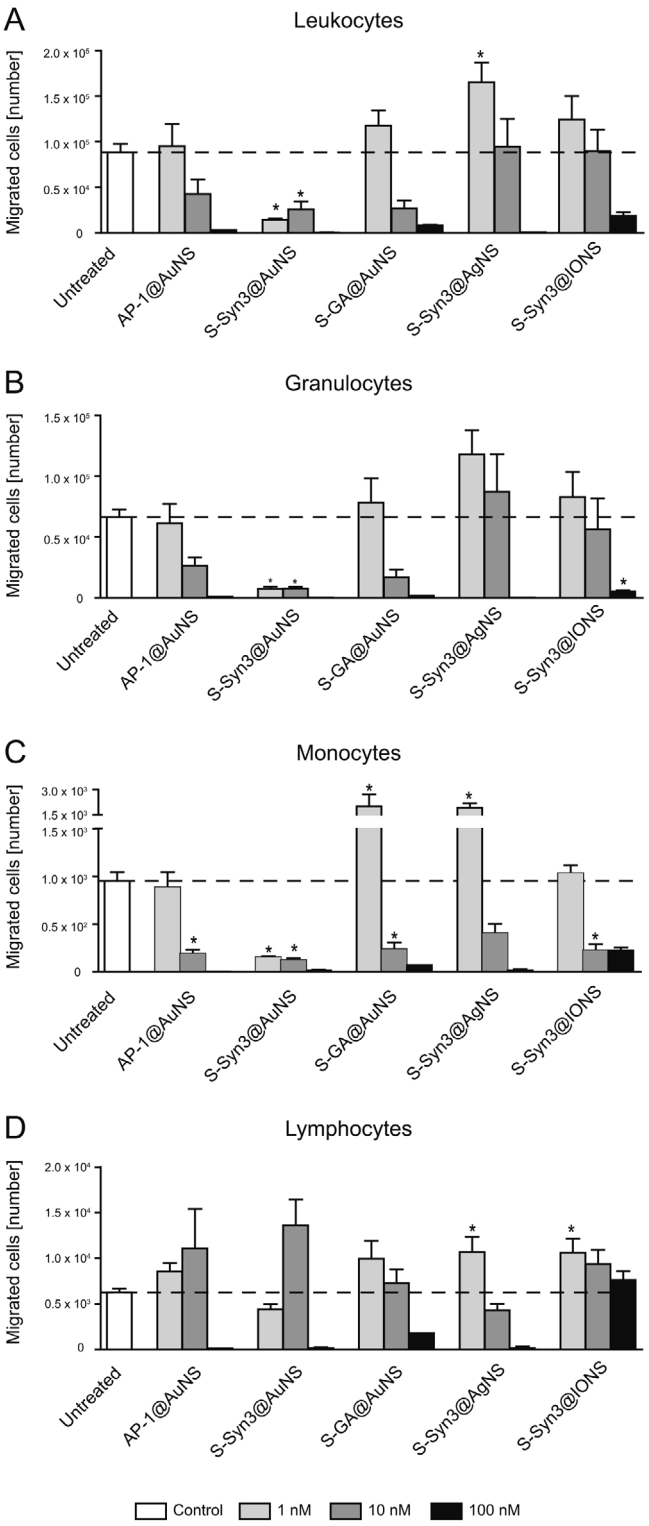

Figure 7. Dose-dependent inhibition of leukocyte migration by nanoparticle endgroups and sulfation. Control AuNS were functionalized with MUDS, the aminopyran-based endgroups were unsulfated AP-1, (AP-1) sulfated Syn3 (S-Syn3), and sulfated glucosamine (S-GA). Further, sulfated Syn3 was also coordinated to AgNS or IONS. Mean data of $n = 4$. $^*p < 0.05$ compared to the untreated control (one way ANOVA).

highly specific and cell-selective control of migration, which can be applied to many different applications. We further outline the complex relations between multivalency, L-selectin binding, and the related consequences on immune cell migration.

A variation of surface chemistry unraveled the fact that pyran and oxepane derivates require an appropriate spatial orientation in order to achieve efficient presentation to selectins. Notably, also an overload with negative charge or higher steric hindrance may affect cell motility.

The comparison of the different particle types functionalized with sulfated Syn3 leads to the conclusion that the core material plays a minor role. Thus, the potential binding properties can be combined with further desirable optical or magnetic properties. We therefore highlight the herein discovered role of the ligand shell for binding on immune cell migration. Using selectins as modulators of immune cell migration might represent a promising approach for immunotherapy and cellular therapy against cancer and inflammatory diseases. In this study, we put a particular emphasis on generating improved selectin-binding nanocarriers, which further make use of the multivalency concept of selectin binding. The obtained results indicate that nanomaterials are suitable scaffolds for the multivalent presentation of carbohydrate mimetics to overcome the comparatively low binding affinity of the monovalent epitopes.

4. Experimental Section

Nanoparticle Generation: Chemicals were purchased from commercial sources and used as received without further purification. All reactions of nanoparticles in aqueous solution were performed in ultrapure water using a 18.2 MΩ, Milli-Q water purification system type ELIX 20 from Millipore Corp. (USA). Organic solvents were distilled before usage. All glassware was thoroughly cleaned with *aqua regia* (3:1 v/v of 37% HCl and 65% HNO_3 solutions), followed by rinsing with ultrapure water. All syntheses of nanoparticles, ligand exchanges, and coupling reactions were conducted under argon atmosphere, using standard Schlenk technique. Purification of the nanoparticles was obtained by multiple steps of dialysis, using cellulose dialysis membrane with a molecular weight cut off (MWCO) of 3.5–5 kDa (Carl Roth GmbH, Germany) or cellulose ester dialysis membrane (MWCO: 3.5–5 kDa; Spectrum Laboratories Inc., USA).

The semiconductor quantum dot synthesis was carried out by a microwave irradiation experiment using a Monowave 300 single-mode microwave reactor (2.45 GHz, 850 W) from Anton Paar GmbH (Austria). The reaction temperature was monitored using an external infrared sensor and an internal fiber-optic (ruby) thermometer. For each synthesis, a 30 mL borosilicate glass reaction vial was used. It was sealed with a snap cap and a standard polytetrafluoroethylene-coated silicone septa. The synthesis was performed at a stirring rate of 600 rpm and simultaneous cooling during the reaction time with compressed air.

Additional details on nanoparticles generation are provided in Supporting Information.

Nanoparticle Characterization: The successful immobilization of epitopes on the particle surfaces was controlled by NMR and IR spectroscopy. All NMR spectra were recorded on an Avance II 400 MHz WB spectrometer of Bruker BioSpin GmbH (Germany). Chemical shifts (δ) are given in ppm relative to tetramethylsilane or the respective solvent peaks. Due to the rigidity of alkyl chains in the thiol shells of functionalized nanoparticles and the resulting large differences in the relaxation times, no integrals are given for the proton NMR data. IR spectra were measured on a Bruker Optics (Germany) IFS48 or on a Bruker Optics IFS25 spectrometer in ATR mode. All optical measurements were performed at room temperature under ambient conditions. UV–vis spectra were recorded with an Agilent 8453 spectrophotometer (Agilent Technologies Inc., USA), whereas emission spectra were recorded with a spectrofluorometer FP8300 from JASCO (Germany), using a xenon lamp and an excitation wavelength of 450 nm. The surface charge of the nanoparticles was determined by zeta potential measurements. The measurements were performed in water with KCl (10 mM) as background electrolyte at 150 mV. The diameters of nanoparticles were determined by DLS measurements and TEM. DLS measurements were performed with a StabiSizer PMX 200C from Particlemetrix (Germany). Samples were irradiated using a red laser, and the intensity fluctuations of the scattered light (detected at a backscattering angle) were analyzed to obtain the autocorrelation function. Hydrodynamic diameter and size distribution were provided by using intensity or number distribution. TEM images were recorded using a Philips CM30 STEM (300 kV, LaB6-cathode) equipped with a GATAN digital camera. TEM samples were prepared by placing a 10 µL drop of the particle sample dispersion onto a carbon film supported copper grid. The mean particle core sizes were determined by measuring at least 100 individual particles from recorded TEM images.

The magnetic properties of the particles in suspension were assessed using an EV7 magnetic vibrating sample magnetometer (VSM) from ADE Technologies (USA). The magnetization curves were measured at room temperature on samples sealed in Teflon vessels and placed on a glass sample holder between two poles of an electromagnet. Elemental concentrations were obtained through inductively coupled plasma optical emission spectrometry using a Horiba Jobin Yvon Ultima 2 (pressure: 2.12 bar; flow: 0.88 L min^{-1}; Au: $\lambda = 242.795$ nm; Fe: $\lambda = 238.204$ nm; Ag: $\lambda = 328.068$ nm). Samples were prepared following established protocols.[37]

Selectin Ligand Binding Assay: Binding of sulfated aminopyran coordinated AuNS to L-selectin was studied by an established protocol for a SPR-based competitive binding assay.[46] First, the binding (detected as resonance units) of selectin-coated AuNS to a standard selectin ligand (20 mol% SLex and 5 mol% sulfotyrosine conjugated to polyacrylamide), immobilized on a sensor chip, was tested. The resulting signal was used as a control (100% binding). The calculated IC_{50} values (half inhibitory concentration) are the molar concentrations of the inhibitor needed to reduce the binding signal to 50% of the initial value.

Isolation, Culture, and Analysis of Endothelial Cells: HUVECs were obtained from Promocell and cultured as previously described.[37] Briefly, 5000 cells were dissolved in 100 µL of endothelial cell growth medium supplemented with vascular endothelial growth factor (ScienCell). In order to remove non-adherent cells, the medium was replaced after 24 h. The cells were cultured on collagen-coated tissue culture treated polystyrol (TCPS) 96-well plates until >80% confluency, which occurs after approximately 48 h. The medium was replaced again and the NS were added at a concentration of 10 nM, and both were incubated on collagen-coated culture plates for 24 h. Cellular viability was analyzed using an MTT assay as published before.[47] An SYTOX Green Dead Cell Stain was also performed.

Immune Cell Isolation: Human primary blood leukocytes were isolated from buffy coats using dextran sedimentation. PBMCs were isolated using Ficoll-based density centrifugation. To isolate monocytes for macrophage culture, PBMC were incubated at 37 °C with 5% human autologous serum for 35 min in a humidified incubator until monocytes became adherent. Non-adherent cells were removed with the supernatant after four times of washing with the medium. Monocytes were cultured for 7 days in RPMI1640 medium supplemented with 5% human autologous serum to obtain macrophages.

Cell Migration Studies: Two million blood leukocytes or one million macrophages were resolved in 1 mL RPMI1640 with 5% FCS in 1.5 mL reaction tubes and were incubated with the nanoparticles and continuous shaking conditions of 500 rpm using a thermomixer (Eppendorf). The concentration of the NS was 1, 10, or 100 nm. Subsequently, cells were centrifuged at 350 *g* for 10 min and resuspended in 200 µL RPMI1640 with 1% FCS for the migration assay. Cells were added on top of the transwell inserts, which contained 800 µL RPMI1640 with 1% FCS in 24-well plates at the plate bottom. Migration assays with blood leukocytes were performed for 1 h, whereas macrophages were allowed to migrate for 16 h at 37 °C in a humidified incubator with CO_2. Following the migration, the inserts were removed after the designated time-points and cells that had migrated

into the bottom were counted using an FACS Canto II (Becton Dickinson) and confirmed using a hemocytometer (disposable Neubauer chamber). Count beads (Calibrite beads, BD) were used to normalize the number of migrated cells in each well. Flow cytometric data were analyzed with FlowJo 7.6.1 software (Treestar, La Jolla, CA).

Statistical Analysis: Data analyses were performed using GraphPad Prism 5.0 software. One way ANOVA with Bonferroni's post-test was done to test significance of data versus untreated control cells. $p < 0.05$ was considered statistically significant ($n = 4$).

Supporting Information

Supporting Information is available from the Wiley Online Library or from the author.

Acknowledgements

This study was supported by the COST Action BM1404 Mye-EUNITER (http://www.mye-euniter.eu), which is part of the European Union Framework Program Horizon 2020 (to MB), the German Research Foundation (6226/2-1, to MB), and an EMBO fellowship (ID 7033) to AMR. The authors would like to thank Léa Bouché (Institute of Chemistry and Biochemistry, Freie Universität Berlin) for the synthesis of the poly(hydroxy)aminooxepane, Anne Schulze for help with TEM (Institute of Inorganic and Analytical Chemistry, Justus-Liebig-University Giessen), and Silvia Rudloff ("Methodenplattform" [http://www.methodenplattform.de]; Institute of Nutritional Science, Justus-Liebig-University Giessen) for experiments with endothelial cells. The authors further thank Micha Gratz (Experimentalphysik, Universität des Saarlandes) for VSM measurements. The authors thank Hans-Ulrich Reissig for help with the selection of aminopyran and poly(hydroxy)aminooxepane ligands. I.T. acknowledges Sabine Schlecht for the initiation of carbohydrate sulfation.

Conflict of Interest

The authors declare no conflict of interest.

Keywords

immunomodulation, macrophages, nanospheres, selectin inhibition, selectin mimetics

Received: July 23, 2019
Revised: September 28, 2019
Published online: October 29, 2019

[1] J. Y. Mary, *Biomed. Pharmacother.* **1985**, *39*, 66.
[2] N. Borregaard, O. E. Sorensen, K. Theilgaard-Monch, *Trends Immunol.* **2007**, *28*, 340.
[3] H. Gussen, P. Hohlstein, M. Bartneck, K. T. Warzecha, L. Buendgens, T. Luedde, C. Trautwein, A. Koch, F. Tacke, *J. Intensive Care* **2019**, *7*, 26.
[4] J. Wang, *Cell Tissue Res.* **2018**, *371*, 531.
[5] M. Bartneck, C. T. Schlosser, M. Barz, R. Zentel, C. Trautwein, T. Lammers, F. Tacke, *ACS Nano* **2017**, *11*, 9689.
[6] M. Bartneck, H. A. Keul, S. Singh, K. Czaja, J. Bornemann, M. Bockstaller, M. Moeller, G. Zwadlo-Klarwasser, J. Groll, *ACS Nano* **2010**, *4*, 3073.
[7] M. Bartneck, H. A. Keul, G. Zwadlo-Klarwasser, J. Groll, *Nano Lett.* **2010**, *10*, 59.
[8] M. Bartneck, T. Ritz, H. A. Keul, M. Wambach, J. Bornemann, U. Gbureck, J. Ehling, T. Lammers, F. Heymann, N. Gassler, T. Ludde, C. Trautwein, J. Groll, F. Tacke, *ACS Nano* **2012**, *6*, 8767.
[9] P. Hohlstein, H. Gussen, M. Bartneck, K. T. Warzecha, C. Roderburg, L. Buendgens, C. Trautwein, A. Koch, F. Tacke, *J. Clin. Med.* **2019**, *8*.
[10] T. A. Springer, *Cell* **1994**, *76*, 301.
[11] V. H. Pomin, *Eur. J. Med. Chem.* **2015**, *92*, 353.
[12] K. E. Moog, M. Barz, M. Bartneck, F. Beceren-Braun, N. Mohr, Z. Wu, L. Braun, J. Dernedde, E. A. Liehn, F. Tacke, T. Lammers, H. Kunz, R. Zentel, *Angew. Chem., Int. Ed.* **2017**, *56*, 1416.
[13] H. Watz, D. Bock, M. Meyer, K. Schierhorn, K. Vollhardt, C. Woischwill, F. Pedersen, A. Kirsten, K. M. Beeh, W. Meyer-Sabellek, H. Magnussen, J. Beier, *Pulm. Pharmacol. Ther.* **2013**, *26*, 265.
[14] T. Wun, M. J. Telen, L. Krishnamurti, T. L. McCavit, L. M. DeCastro, H. Flanner, F. A. Kuypers, S. K. Larkin, S. Rhee, J. L. Magnani, H. M. Thackray, *Blood* **2014**, *124*, 2704.
[15] H. W. Chiu, L. H. Li, C. Y. Hsieh, Y. K. Rao, F. H. Chen, A. Chen, S. M. Ka, K. F. Hua, *Sci. Rep.* **2019**, *9*, 5603.
[16] W. I. Weis, K. Drickamer, *Annu. Rev. Biochem.* **1996**, *65*, 441.
[17] C. Fasting, C. A. Schalley, M. Weber, O. Seitz, S. Hecht, B. Koksch, J. Dernedde, C. Graf, E. W. Knapp, R. Haag, *Angew. Chem., Int. Ed.* **2012**, *51*, 10472.
[18] J. J. Lundquist, E. J. Toone, *Chem. Rev.* **2002**, *102*, 555.
[19] L. L. Kiessling, J. E. Gestwicki, L. E. Strong, *Angew. Chem., Int. Ed.* **2006**, *45*, 2348.
[20] D. Barros, S. A. Costa Lima, A. Cordeiro-da-Silva, *Nanomedicine* **2015**, *10*, 387.
[21] R. P. McEver, *Cardiovasc. Res.* **2015**, *107*, 331.
[22] J. Dernedde, I. Papp, S. Enders, S. Wedepohl, F. Paulus, R. Haag, *J. Carbohydr. Chem.* **2011**, *30*, 347.
[23] L. Bouché, H.-U. Reissig, *Eur. J. Org. Chem.* **2014**, *2014*, 3697.
[24] J. Salta, J. Dernedde, H. U. Reissig, *Beilstein J. Org. Chem.* **2015**, *11*, 638.
[25] L. Bouche, M. Kandziora, H. U. Reissig, *Beilstein J. Org. Chem.* **2014**, *10*, 213.
[26] M. Roskamp, S. Enders, F. Pfrengle, S. Yekta, V. Dekaris, J. Dernedde, H. U. Reissig, S. Schlecht, *Org. Biomol. Chem.* **2011**, *9*, 7448.
[27] F. Pfrengle, H. U. Reissig, *Chem. Eur. J.* **2010**, *16*, 11915.
[28] A. Al-Harrasi, H. U. Reissig, *Angew. Chem., Int. Ed.* **2005**, *44*, 6227.
[29] M. Kandziora, H. U. Reissig, *Beilstein J. Org. Chem.* **2014**, *10*, 1749.
[30] M. Kandziora, E. Mucha, S. P. Zucker, H.-U. Reissig, *Synlett* **2015**, *26*, 367.
[31] N. Desai, *AAPS J.* **2012**, *14*, 282.
[32] Y. Tsvetkova, N. Beztsinna, M. Baues, D. Klein, A. Rix, S. K. Golombek, W. Al Rawashdeh, F. Gremse, M. Barz, K. Koynov, S. Banala, W. Lederle, T. Lammers, F. Kiessling, *Nano Lett.* **2017**, *17*, 4665.
[33] G. Wang, M. R. Papasani, P. Cheguru, P. J. Hrdlicka, R. A. Hill, *Nanomedicine* **2012**, *8*, 822.
[34] E. Casals, T. Pfaller, A. Duschl, G. J. Oostingh, V. Puntes, *ACS Nano* **2010**, *4*, 3623.
[35] M. J. Hostetler, J. E. Wingate, C.-J. Zhong, J. E. Harris, R. W. Vachet, M. R. Clark, J. D. Londono, S. J. Green, J. J. Stokes, G. D. Wignall, G. L. Glish, M. D. Porter, N. D. Evans, R. W. Murray, *Langmuir* **1998**, *14*, 17.
[36] Y. M. Cho, Y. Mizuta, J. I. Akagi, T. Toyoda, M. Sone, K. Ogawa, *J. Toxicol. Pathol.* **2018**, *31*, 73.
[37] M. Bartneck, H. A. Keul, M. Wambach, J. Bornemann, U. Gbureck, N. Chatain, S. Neuss, F. Tacke, J. Groll, G. Zwadlo-Klarwasser, *Nanomedicine* **2012**, *8*, 1282.
[38] H. Xu, A. Manivannan, I. Crane, R. Dawson, J. Liversidge, *Blood* **2008**, *112*, 1166.
[39] V. Brinkmann, U. Reichard, C. Goosmann, B. Fauler, Y. Uhlemann, D. S. Weiss, Y. Weinrauch, A. Zychlinsky, *Science* **2004**, *303*, 1532.

[40] W. Gross-Weege, M. Weiss, M. Schneider, M. Wenning, B. Harms, K. Dumon, C. Ohmann, H. D. Roher, *Intensive Care Med.* **1997**, *23*, 16.
[41] S. Zanganeh, G. Hutter, R. Spitler, O. Lenkov, M. Mahmoudi, A. Shaw, J. S. Pajarinen, H. Nejadnik, S. Goodman, M. Moseley, L. M. Coussens, H. E. Daldrup-Link, *Nat. Nanotechnol.* **2016**, *11*, 986.
[42] V. Kumar, L. Donthireddy, D. Marvel, T. Condamine, F. Wang, S. Lavilla-Alonso, A. Hashimoto, P. Vonteddu, R. Behera, M. A. Goins, C. Mulligan, B. Nam, N. Hockstein, F. Denstman, S. Shakamuri, D. W. Speicher, A. T. Weeraratna, T. Chao, R. H. Vonderheide, L. R. Languino, P. Ordentlich, Q. Liu, X. Xu, A. Lo, E. Pure, C. Zhang, A. Loboda, M. A. Sepulveda, L. A. Snyder, D. I. Gabrilovich, *Cancer Cell* **2017**, *32*, 654.
[43] S. Epelman, K. J. Lavine, G. J. Randolph, *Immunity* **2014**, *41*, 21.
[44] M. Bartneck, K. H. Heffels, Y. Pan, M. Bovi, G. Zwadlo-Klarwasser, J. Groll, *Biomaterials* **2012**, *33*, 4136.
[45] S. Gu, T. Ni, J. Wang, Y. Liu, Q. Fan, Y. Wang, T. Huang, Y. Chu, X. Sun, *J. Immunol. Res.* **2018**, *2018*, 6156757.
[46] S. Enders, G. Bernhard, A. Zakrzewicz, R. Tauber, *Biochim. Biophys. Acta, Gen. Subj.* **2007**, *1770*, 1441.
[47] M. Bartneck, F. M. Peters, K. T. Warzecha, M. Bienert, L. van Bloois, C. Trautwein, T. Lammers, F. Tacke, *Nanomedicine* **2014**, *10*, 1209.